# Eddy Currents in an Infinite Slab due to an Elliptic Current Excitation

Stavros M. Panas and Antonis G. Papayiannakis

*Abstract*—**The magnetic flux density and the eddy-current density induced in a conducting plate of finite thickness by an elliptic filamentary current loop parallel to the slab are calculated. The system of coordinates used is the Cartesian one, and as a result, the method can be applied to any filamentary excitation parallel to the slab interface once the excitation is expressed in the Cartesian system of coordinates. The solution of the partial differential equations describing the problem is achieved by 2D spatial Fourier transformation, and the final inverse transformation is performed by applying the 2D fast inverse Fourier transform. The displacement current is not neglected as is usually done, and therefore the method can be applied to low and high excitation frequencies. The method can be easily extended to cover the case of multiple layers, and it can be applied to problems ranging from power applications to eddy-current nondestructive testing.**

## I. Introduction

THE problem of calculating the eddy-current distribution and the associated power losses induced in a conducting semi-infinite slab or a plate of finite thickness have been examined for various forms of filamentary excitation current loops [1]–[10]. In the case of eddy-current nondestructive testing, the change of the complex impedance of both the excitation and the search coil is a quantity of interest for characterizing the defects within the conducting slab.

Depending on the position of the excitation current relative to the slab/plate, three categories of problems exist. To the first category belong the configurations where the excitation is placed parallel to the face of the slab, as is the case of a circular loop placed parallel to a semi-infinite slab [1] or parallel to a plate of finite thickness [2] and the case of a rectangular [3] or circular [7] loop moving parallel to a conducting slab. To the second category belong the configurations where the excitation is lying on a plane perpendicular to the slab, as is the case of a circular loop perpendicular to a semi-infinite slab in steady-state [4] or transient [5] conditions. Finally, the third category comprises the more general case of an excitation lying on a plane oblique to the plate, such as a circular loop placed at an arbitrary position above a conducting plate [6], [8].

All of the above forms of excitation are of great interest in areas ranging from power applications such as the case of rotating machines [1] and the calculation of forces on moving loops [7] to the information extraction processes, as is the case of ac nondestructive testing [10].

The methods of treating the problem in the early literature were ingenious. But the small computing power of those days compared to today's great computing power of even small PC's was a major handicap for obtaining numerical solutions as functions of the various parameters of the problem.

Usually, the field equations are expressed in terms of the magnetic vector potential (MVP) from which the magnetic flux density, the eddy-current density, the power losses, and the forces can be easily obtained. A necessary step towards the calculation of the MVP is the calculation of integrals in one, two, or three variables (depending on the form of the excitation) which must be performed numerically. This is a crucial step, and many methods of integration have been introduced. We must emphasize the fact that the integration must be performed for every $(x, y, z)$ point where a field quantity must be evaluated. If, additionally, the influence of the geometric (distance between excitation current and conducting slab, radius of the loop, etc.) and/or electromagnetic parameters (resistivity, conductivity) must be examined, the integration has to be repeated for the same $(x, y, z)$ point every time one of the parameters attains a different value.

In this work, we will consider the case of an elliptic filamentary current loop placed above a conducting plate of finite thickness and parallel to the surface of the plate. For this configuration, we will calculate the eddy-current density and the power loss inside the plate and the magnetic flux density in the plate and in the air. The formulation that will be adopted for the solution is not restricted to the case of the elliptic loop only. As will be shown, any excitation parallel to the plate can be considered as input to the formulas calculating the desired quantities, even if the current loop considered is not a closed one, but extends to infinity, as in the case of current sheets or infinite current lines. The only restriction that exists is that the excitation current must be expressed in Cartesian coordinates.

Before we proceed with our analysis, some comments on the existing methodology and techniques appearing in the literature will follow.

*1) System of Coordinates:* The system of coordinates used in [1] for the formulation of the equations is the cy-

Manuscript received July 25, 1990; revised March 14, 1991.

The authors are with the School of Electrical Engineering, Aristotle University of Thessaloniki, GR-54 006, Thessaloniki, Greece.

IEEE Log Number 9100959.

lindrical one. This system is quite useful for the case of circular coils placed parallel to the slab. For coils of different geometries like rectangular or elliptical ones, the system of coordinates shoud be, respectively, Cartesian or elliptical. The Cartesian system is also used for vertical coils or coils oblique to the slab. Looking for a coordinate system that is applicable to all three kinds of coils in various orientations, the Cartesian one seems to be more adequate. The expression for a rectangular filamentary loop in Cartesian coordinates is obtained easily, but for the case of an elliptical loop, the procedure is quite tedious. Fortunately, once it is obtained, it also can be used for the case of circular coils by equating the small and large axes of the ellipse. If we want to investigate the eddy-current density and magnetic flux density arising from a combination of filamentary excitations having different geometries and lying on the same or on different planes parallel to the conducting plate, superposition can be applied.

*2) Solution of the Partial Differential Equations:* Let us elaborate on the approach followed by Hammond [1] for the calculation of the MVP in the case of a semi-infinite slab. In his work, the MVP inside and outside the slab is calculated through the numerical evaluation of finite integrals with limits from zero to infinity. For the evaluation of these integrals, two limiting cases are considered based on the value of the quantity $k\mu_r$ where $\mu_r$ is the relative permeability of the slab and $k$ is the variable of integration ranging from zero to infinity. These limiting cases simplify the evaluation of the integrals and lead to the resistance-limited case for

$$k\mu_r \gg \text{Real } \{\sqrt{k^2 + jp^2}\}$$

and to the inductance-limited case for

$$k\mu_r \ll p$$

where $p^2 = \mu\omega a^2/\rho$, $\mu$ and $\rho$ are, respectively, the permeability and the resistivity of the slab, $\omega$ is the angular frequency of the excitation, and $a$ is the radius of the current loop.

Let us comment now on these two limiting cases. For constant geometry, angular frequency, resistivity, and permeability of the conducting slab, the above equations are functions of the variable $k$ only. Since the range of values of $k$ is from zero to infinity, the numerical evaluation of the integrals along a finite band of $k$ introduces a truncation error. Keeping in mind that the lower limit of integration is $k = 0$, it is obvious that for a range of small $k$ around $k = 0$, the first of the above equations never holds. This problem can be overcome by considering the lower limit of $k$ to be small, but greater than zero, for instance, $k = 1/4$ as in [1]. There are also some restrictions for this equation to be valid. These restrictions have to do with the material of the slab and the radius of the loop. Thus, the resistance-limited approximation is valid in the case of unsaturated iron and a loop radius on the order of 1 cm.

In the inductance-limited case, for the second of the above equations to hold, we must impose an upper bound on $k$. This bound depends on the magnetic permeability of the slab, the radius of the loop, and the distance of the coil from the slab. This equation is valid for nonmagnetic materials and a coil radius on the order of 10 cm or saturated iron and coils of radius on the order of 1 m. The same classification into resistance- and inductance-limited cases is followed in almost all other works dealing with the subject.

The above-mentioned categorization yields a very helpful engineering design method by leading to approximations of the integrals according to the relative values of various dimensionless factors such as $\mu_r$, $p$, and $b/a$ ($b$ is the distance of the coil from the slab).

It is the opinion of the authors of this paper that a numerical evaluation of the integrals that give the MVP without any simplification arising from resistance- or inductance-limited considerations would be a more desired one. In such a case, the notions of resistance- and inductance-limited inequalities would be of great help in establishing the limits of the numerical integration and in relating the aforementioned dimensionless factors to design problems.

## II. The Magnetic Vector Potential

The geometrical configuration of the problem is shown in Fig. 1. An elliptical line current $\bar{J}$ is situated parallel and at a distance $h$ from the upper surface of a slab of thickness $d$. The upper surface of the slab coincides with the $x$–$y$ plane at $z = 0$. The infinite space is thus divided into four layers, $i = 1, 2, 3, 4$ with plane separating surfaces parallel to the $x$–$y$ plane, the numbering starting from the top towards $(-z)$.

A harmonic time dependence of the form exp $\{+j\omega t\}$ is assumed and hereafter suppressed. The Coulomb gauge condition is also imposed on the magnetic vector potential (MVP) within each layer:

$$\nabla \cdot \bar{A}_i = 0, \qquad i = 1, 2, 3, 4 \tag{1a}$$

with a choice of zero scalar electric potential

$$\varphi_i = 0, \qquad i = 1, 2, 3, 4 \tag{1b}$$

implying that the volume charge distribution within the layers is also zero:

$$\rho_i = 0, \qquad i = 1, 2, 3, 4. \tag{1c}$$

The volume current distributions within the layers are also supposed to be zero.

With the above assumptions, the field vectors are expressed with respect to the MVP within each layer as

$$\bar{E}_i = -j\omega\bar{A}_i, \qquad i = 1, 2, 3, 4 \tag{2a}$$

$$\bar{B}_i = \nabla \times \bar{A}_i, \qquad i = 1, 2, 3, 4 \tag{2b}$$

and the MVP within the layers is a solution of the Helmholtz equation

$$\nabla^2\bar{A}_i + k_i^2\bar{A}_i = 0, \qquad i = 1, 2, 3, 4 \tag{3}$$

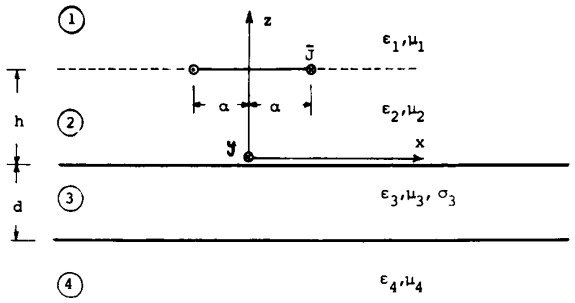


Fig. 1. Geometry of the problem.

where $k_i$ is the wavenumber of the respective layer medium:

$$k_i^2 = \omega^2 \mu_i \epsilon_i, \qquad i = 1, 2, 4 \tag{4a}$$

$$k_3^2 = \mu^2 \mu_3 \epsilon_3 - j\omega\mu_3\sigma_3. \tag{4b}$$

Since there is no $z$ component of the excitation current and the extent of the media is infinite along the $x$–$y$ plane, it follows that the $z$ component of the MVP is also zero:

$$A_z = \tilde{A}_z = 0. \tag{5}$$

Applying the spatial two-dimensional Fourier transform (2D FT) with respect to $x$ and $y$ in (3) yields, for each Cartesian component of the MVP,

$$\frac{\partial^2 \tilde{A}_{ip}}{\partial z^2} + \lambda_i^2 \tilde{A}_{ip} = 0, \qquad p = x, y, \qquad i = 1, 2, 3, 4 \tag{6}$$

where

$$\tilde{A}_{ip} = \mathfrak{F}_{xy}\{A_{ip}\} = \mathfrak{F}_x \mathfrak{F}_y \{A_{ip}\} \tag{7}$$

and $\lambda_i$ is the eigenvalue connected to the spatial angular frequency eigenvalues $\kappa_x$ and $\kappa_y$ by the relations

$$\lambda_i^2 = k_i^2 - (\kappa_x^2 + \kappa_y^2) \tag{8a}$$

$$\kappa_x^2 + \kappa_y^2 \in \mathbb{R}, \qquad \mathrm{Re}\,\{\lambda_i\} > 0, \ \mathrm{Im}\,\{\lambda_i\} \leqslant 0. \tag{8b}$$

The solution of (6) has the form

$$\tilde{A}_{ip} = C_{ip} e^{-j\lambda_i z} + D_{ip} e^{+j\lambda_i z} \tag{9}$$

with a derivative

$$\frac{\partial \tilde{A}_{ip}}{\partial z} = -j\lambda_i [C_{ip} e^{-j\lambda_i z} - D_{ip} e^{+j\lambda_i z}]. \tag{10}$$

The appropriate boundary conditions for the computation of the $C_{ip}$ and $D_{ip}$ integration constants are as follows.

• The radiation condition for $|z| \to \infty$

$$\lim_{|z|\to\infty} \left[\frac{\partial A_{ip}}{\partial |z|} + j\lambda_i A_{ip}\right] = 0, \qquad i = 1, 4 \tag{11}$$

which, after Fourier transforming and interchanging the order of the limit and integration operators, gives

$$\lim_{|z|\to\infty} \left[\frac{\partial \tilde{A}_{ip}}{\partial |z|} + j\lambda_i \tilde{A}_{ip}\right] = 0, \qquad i = 1, 4. \tag{12}$$

•The boundary conditions of the field vectors on the layer interfaces

$$\hat{z}_0 \times (\bar{E}_i - \bar{E}_{i+1}) = 0 \tag{13a}$$

$$\hat{z}_0 \times (\bar{H}_i - \bar{H}_{i+1}) = \bar{J}_{si} \tag{13b}$$

for $i = 1, 2, 3$, which give the following boundary conditions for the MVP:

$$\hat{z}_0 \times \bar{A}_i - \hat{z}_0 \times \bar{A}_{i+1} = 0 \tag{14a}$$

$$\frac{1}{\mu_i} \hat{z}_0 \times \nabla \times \bar{A}_i - \frac{1}{\mu_{i+1}} \hat{z}_0 \times \nabla \times \bar{A}_{i+1} = \bar{J}_{si} \tag{14b}$$

where $\bar{J}_{si}$ is the surface current distribution impressed on the discontinuity surface between the layers $i$ and $i + 1$ with

$$\bar{J}_{si} = \bar{J}, \qquad i = 1 \tag{15a}$$

$$\bar{J}_{si} = 0, \qquad i = 2, 3. \tag{15b}$$

Expressing (14) in terms of the MVP Cartesian components and again applying a 2-D spatial FT yields the equations

$$\tilde{A}_{ip} = \tilde{A}_{i+1,p} \tag{16a}$$

$$\frac{1}{\mu_i} \frac{\tilde{A}_{ip}}{\partial z} - \frac{1}{\mu_{i+1}} \frac{\partial \tilde{A}_{i+1,p}}{\partial z} = -\tilde{J}_{si,p} \tag{16b}$$

for $p = x, y$ and $i = 1, 2, 3$.

Application of the radiation condition of (12) to the $x$ and $y$ components of the MVP in layer 1 from (9) and (10) as $z \to +\infty$ gives finally

$$D_{1x} = D_{1y} = 0. \tag{17a}$$

Application of the radiation condition of (12) to the $x$ and $y$ components of the MVP in layer 4 from (9) and (10) as $z \to -\infty$ gives finally

$$C_{4x} = C_{4y} = 0. \tag{17b}$$

Application of (15) and (16) at the discontinuity surfaces between the layers forms two $6 \times 6$ uncoupled linear algebraic systems, one for the $x$ components of the MVP, and one for the $y$ components. The solution of these two systems yields, for the integration constants $C_{ip}$, $D_{ip}$, $i = 1, 2, 3, 4$ for $p = x$ and $p = y$,

$$C_{1p} = \left\{\frac{\mu_0}{2j\lambda_0}(e^{+j\lambda_0 h} - e^{-j\lambda_0 h}) - [(\lambda_3\mu_0 - \lambda_0\mu_3)e^{-j\lambda_3 d} + (\lambda_3\mu_0 + \lambda_0\mu_3)e^{+j\lambda_3 d}]\,Q\right\}\tilde{J}_p \tag{17c}$$

$$C_{2p} = \left\{-\frac{\mu_0}{2j\lambda_0} e^{-j\lambda_0 h} - [(\lambda_3\mu_0 - \lambda_0\mu_3)e^{-j\lambda_3 d} + (\lambda_3\mu_0 + \lambda_0\mu_3)e^{+j\lambda_3 d}]\,Q\right\}\tilde{J}_p \tag{17d}$$

$$C_{3p} = -j(\lambda_3\mu_0 - \lambda_0\mu_3)e^{-j\lambda_3 d} Q \tilde{J}_p \tag{17e}$$

$$D_{zp} = \frac{\mu_0}{2j\lambda_0} e^{-j\lambda_0 h} \tilde{J}_p \tag{17f}$$

$$D_{3p} = -j(\lambda_3\mu_0 + \lambda_0\mu_3) e^{+j\lambda_3 d} Q \tilde{J}_p \tag{17g}$$

$$D_{4p} = -2j\lambda_3\mu_0 e^{+j\lambda_0 d} Q \tilde{J}_p \tag{17h}$$

$$Q = \frac{-\mu_3\mu_0 e^{-j\lambda_0 h}}{(\lambda_3\mu_0 - \lambda_0\mu_3)^2 e^{-j\lambda_3 d} - (\lambda_3\mu_0 + \lambda_0\mu_3)^2 e^{+j\lambda_3 d}}. \tag{17i}$$

## III. The Excitation Current

In order to use the above expressions of (17), the FT of the excitation current must be computed. The complex form of the excitation current can be represented as [11]

$$\bar{J} = I\delta_l \hat{l}_0 \tag{18}$$

where

- $\bar{J}$ [A/m$^2$] volume current distribution of the excitation
- $I$ [A] magnitude of the line current
- $\delta_l$ [m$^{-2}$] Dirac delta function describing the elliptical curve of the current flow
- $\hat{l}_0$ unit vector tangential to the curve of the ellipse and having the direction of the current flow.

The curve Dirac delta $\delta_l$ must be such that

$$\delta_l = 0 \tag{19a}$$

for any point not on the ellipse curve, and

$$\int_S \bar{J} \cdot d\bar{s} = I \tag{19b}$$

on any surface $S$ perpendicularly intersecting the ellipse curve.

The ellipse curve described by the equations

$$\frac{x^2}{a^2} + \frac{y^2}{b^2} = 1 \tag{20a}$$

$$z = h \tag{20b}$$

can be considered as the intersection of two families of surfaces: the planes

$$u_1 = z - h \tag{21a}$$

and the elliptical cylinders

$$u_2 = \frac{x^2}{a^2} + \frac{y^2}{b^2} - 1 \tag{21b}$$

for $u_1 = u_2 = 0$.

Then the desired Dirac delta function is given by

$$\delta_l = |\nabla u_1 \times \nabla u_2|\, \delta(u_1)\, \delta(u_2). \tag{22}$$

And since the unit vector tangent to the ellipse is

$$\hat{l}_0 = \frac{\nabla u_1 \times \nabla u_2}{|\nabla u_1 \times \nabla u_2|} \tag{23}$$

it yields

$$\delta_l \hat{l}_0 = (\nabla u_1 \times \nabla u_2)\, \delta(u_1)\, \delta(u_2). \tag{24}$$

For $\delta(u_2)$, we use the property of the delta function [12]

$$\delta[f(x, y)] = \sum_j \frac{\delta(x - x_j)}{|f'_x(x_j)|}, \quad \text{for } f(x_j) = 0, f'_x(x_j) \neq 0 \tag{25a}$$

$$= \sum_j \frac{\delta(y - y_j)}{|f'_y(y_j)|}, \quad \text{for } f(y_j) = 0, f'_y(y_j) \neq 0. \tag{25b}$$

The roots of the function $u_2 = f(x, y) = 0$ from (21b) are

$$x_j = \pm\frac{a}{b}\sqrt{b^2 - y^2} \text{ with } |y| \leqslant b, \quad \text{for } j = 1, 2 \tag{26a}$$

with respect to $x$, and

$$y_j = \pm\frac{b}{a}\sqrt{a^2 - x^2} \text{ with } |x| \leqslant a, \quad \text{for } j = 1, 2 \tag{26b}$$

with respect to $y$.

Hence, from (25a) and (26a),

$$\begin{aligned}\bar{J} = I\,\delta_l \hat{l}_0 = I\,\delta(z - h)\Pi\left(\frac{y}{2b}\right) \times \Bigg\{ &-\frac{a}{b}\frac{y}{\sqrt{b^2 - y^2}}\left[\delta\left(x - \frac{a}{b}\sqrt{b^2 - y^2}\right) + \delta\left(x + \frac{a}{b}\sqrt{b^2 - y^2}\right)\right]\hat{x}_0 \\ &+ \left[\delta\left(x - \frac{a}{b}\sqrt{b^2 - y^2}\right) - \delta\left(x + \frac{a}{b}\sqrt{b^2 - y^2}\right)\right]\hat{y}_0\Bigg\}.\end{aligned} \tag{27a}$$

Or, equivalently, from (25b) and (26b),

$$\begin{aligned}\bar{J} = I\,\delta_l \hat{l}_0 = I\,\delta(z - h)\Pi\left(\frac{x}{2a}\right) \times \Bigg\{ &-\left[\delta\left(y - \frac{b}{a}\sqrt{a^2 - x^2}\right) - \delta\left(y + \frac{b}{a}\sqrt{a^2 - x^2}\right)\right]\hat{x}_0 \\ &+ \frac{b}{a}\frac{x}{\sqrt{a^2 - x^2}}\left[\delta\left(y - \frac{b}{a}\sqrt{a^2 - x^2}\right) + \delta\left(y + \frac{b}{a}\sqrt{a^2 - x^2}\right)\right]\hat{y}_0\Bigg\}.\end{aligned} \tag{27b}$$

Now, since

$$\bar{J} = I\,\delta_l \hat{l}_0 = J_x \hat{x}_0 + J_y \hat{y}_0, \tag{28}$$

the 2-D FT of the current density $x$ component is evaluated from (27b) to

$$\tilde{J}_x = j4I\,\delta(z-h)\int_0^{+a} \cos(\kappa_x x)\sin\left(\frac{b}{a}\sqrt{a^2-x^2}\,\kappa_y\right)dx. \tag{29}$$

Similarly, for the $y$ component, we find from (27a)

$$\tilde{J}_y = -j4I\,\delta(z-h)\int_0^{+b} \cos(\kappa_y y) \cdot \sin\left(\frac{a}{b}\sqrt{b^2-y^2}\,\kappa_x\right)dy. \tag{30}$$

From the evaluation carried out in the Appendix, the excitation current transforms finally take the compact form

$$\tilde{J}_x = -j\kappa_y H_0 \tag{31a}$$

$$\tilde{J}_y = +j\kappa_x H_0 \tag{31b}$$

where

$$H_0 = \pi abI[J_0(\sqrt{(a\kappa_x)^2+(b\kappa_y)^2}) + J_2(\sqrt{(a\kappa_x)^2+(b\kappa_y)^2})]\,\delta(z-h). \tag{31c}$$

From (31), it is easily seen that the following property holds:

$$\kappa_x \tilde{J}_x + \kappa_y \tilde{J}_y = 0. \tag{32}$$

The above equation actually expresses the continuity equation in the spatial frequency domain.

## IV. The Transfer Function

Observing (9) and (17), we can see that the FT of the MVP components can be written as

$$\left.\begin{aligned}\tilde{A}_{ix} &= \tilde{H}_i \tilde{J}_x\\ \tilde{A}_{iy} &= \tilde{H}_i \tilde{J}_y\end{aligned}\right\} \quad i = 1, 2, 3, 4 \tag{33}$$

where $\tilde{H}_i$ represents the transfer function of the layer $i$ with

$$\tilde{H}_1 = -\frac{\mu_0}{2j\lambda_0}(e^{-j\lambda_0(z+h)} - e^{-j\lambda_0(z-h)}) - Q[(\lambda_3\mu_0 - \lambda_0\mu_3)e^{-j\lambda_3 d} + (\lambda_3\mu_0 + \lambda_0\mu_3)e^{+j\lambda_3 d}]e^{-j\lambda_0 z} \tag{34a}$$

$$\tilde{H}_2 = -\frac{\mu_0}{2j\lambda_0}(e^{-j\lambda_0(z+h)} - e^{+j\lambda_0(z-h)}) - Q[(\lambda_3\mu_0 - \lambda_0\mu_3)e^{-j\lambda_3 d} + (\lambda_3\mu_0 + \lambda_0\mu_3)e^{+j\lambda_3 d}]e^{-j\lambda_0 z} \tag{34b}$$

$$\tilde{H}_3 = -jQ[(\lambda_3\mu_0 - \lambda_0\mu_3)e^{-j\lambda_3(z+d)} + (\lambda_3\mu_0 + \lambda_0\mu_3)e^{+j\lambda_3(z+d)}] \tag{34c}$$

$$\tilde{H}_4 = -2j\lambda_3\mu_0 Q e^{+j\lambda_0(z+d)}$$

$$Q = \frac{-\mu_3\mu_0 e^{-j\lambda_0 h}}{(\lambda_3\mu_0 - \lambda_0\mu_3)^2 e^{-j\lambda_3 d} - (\lambda_3\mu_0 + \lambda_0\mu_3)^2 e^{+j\lambda_3 d}}. \tag{35e}$$

The derivatives of the layer transfer functions with respect to $z$ are

$$\frac{d\tilde{H}_1}{dz} = \frac{\mu_0}{2}(e^{-j\lambda_0(z+h)} - e^{-j\lambda_0(z-h)}) + j\lambda_0 Q[(\lambda_3\mu_0 - \lambda_0\mu_3)e^{-j\lambda_3 d} + (\lambda_3\mu_0 + \lambda_0\mu_3)e^{+j\lambda_3 d}]e^{-j\lambda_0 z} \tag{36a}$$

$$\frac{d\tilde{H}_2}{dz} = \frac{\mu_0}{2}(e^{-j\lambda_0(z+h)} + e^{+j\lambda_0(z-h)}) + j\lambda_0 Q[(\lambda_3\mu_0 - \lambda_0\mu_3)e^{-j\lambda_3 d} + (\lambda_3\mu_0 + \lambda_0\mu_3)e^{+j\lambda_3 d}]e^{-j\lambda_0 z} \tag{36b}$$

$$\frac{d\tilde{H}_3}{dz} = -\lambda_3 Q[(\lambda_3\mu_0 - \lambda_0\mu_3)e^{-j\lambda_3(z+h)} - (\lambda_3\mu_0 + \lambda_0\mu_3)e^{+j\lambda_3(z+d)}] \tag{36c}$$

$$\frac{d\tilde{H}_4}{dz} = 2j\lambda_0\lambda_3\mu_0 Q e^{+j\lambda_0(z+d)}. \tag{36d}$$

## V. The Field Quantities

As a result, the magnetic induction from (2b) after Fourier transforming and with the use of (33) is given by

$$\tilde{B}_{ix} = -\frac{d\tilde{H}_i}{dz}\tilde{J}_y \tag{37a}$$

$$\tilde{B}_{iy} = +\frac{d\tilde{H}_i}{dz}\tilde{J}_x \tag{37b}$$

$$\tilde{B}_{iz} = j\tilde{H}_i(\kappa_x \tilde{J}_y - \kappa_y \tilde{J}_x) \tag{37c}$$

and using (31),

$$\tilde{B}_{ix} = -j\kappa_x H_0 \frac{d\tilde{H}_i}{dz} \tag{38a}$$

$$\tilde{B}_{iy} = -j\kappa_y H_0 \frac{d\tilde{H}_i}{dz} \tag{38b}$$

$$\tilde{B}_{iz} = -(\kappa_x^2 + \kappa_y^2)H_0\tilde{H}_i. \tag{38c}$$

The electric field intensity vector components within the layers are given from (2a) after Fourier transforming and with the use of (33) by the expressions

$$\tilde{E}_{ip} = -j\omega\tilde{H}_i\tilde{J}_p \tag{39}$$

for $p = x, y$ and $i = 1, 2, 3, 4$, while using (31), they become

$$\tilde{E}_{ix} = -\omega\kappa_y H_0\tilde{H}_i \tag{40a}$$

$$\tilde{E}_{iy} = +\omega\kappa_x H_0\tilde{H}_i. \tag{40b}$$

Within the slab (layer 3), an eddy current volume density is induced, the FT of which is given in a similar manner by

$$\tilde{J}_{3p} = \sigma_3 H_0 \tilde{E}_{3p}, \qquad p = x, y \tag{41}$$

or

$$\tilde{J}_{3x} = -\omega\kappa_y \sigma_3 H_0 \tilde{H}_3 \tag{42a}$$

$$\tilde{J}_{3y} = +\omega\kappa_x \sigma_3 H_0 \tilde{H}_3. \tag{42b}$$

The inverse FT of (38), (40), and (42) with the use of (31c), (35) and (36) gives the complex form of the respective field quantities as a function of the $x$, $y$, $z$ coordinates.

## VI. Numerical Treatment and Results

The two-dimensional inverse Fourier transform (2D IFT) of (38), (40), (42) is performed numerically through the application of the two-dimensional inverse discrete Fourier transform (2D IDFT). The evaluation of the 2D IDFT is made using the two-dimensional inverse fast Fourier transform (2D IFFT) algorithm [13].

The procedure used for the 2D IDFT calculation is briefly presented. Assume that we have to find the 2D IFT $f = f(x, y)$ of the function $\tilde{F} = \tilde{F}(\kappa_x, \kappa_y)$ where $\tilde{F}$ identifies with the Fourier-transformed functions in (38), (40), (42). The function $\tilde{F}(\kappa_x, \kappa_y)$ in our case is not band limited in $\kappa_x$ and $\kappa_y$, and the associated function $f(x, y)$ is not space limited in $x$ and $y$. The various forms of the function $\tilde{F}(\kappa_x, \kappa_y)$ that appear in (38), (40), (42) also possess certain symmetries (even or odd) with respect to $\kappa_x$ or $\kappa_y$ which lead to analogous symmetries in the function $f(x, y)$ with respect to $x$ or $y$.

In order to calculate the 2D IDFT, we first truncate the function $\tilde{F}(\kappa_x, \kappa_y)$ in both $\kappa_x$ and $\kappa_y$ by multiplying it with a 2D rectangular window $W(\kappa_x, \kappa_y)$ where

$$W(\kappa_x, \kappa_y) = \begin{cases} 1, & \text{for } |\kappa_x| \leqslant K_x,\ |\kappa_y| \leqslant K_y \\ 0, & \text{elsewhere} \end{cases} \tag{43}$$

and so we obtain an estimate

$$\hat{F}(\kappa_x, \kappa_y) = \tilde{F}(\kappa_x, \kappa_y) W(\kappa_x, \kappa_y). \tag{44}$$

We then sample the estimate in $\kappa_x$ and $\kappa_y$ with sampling intervals $\Delta F_x$ and $\Delta F_y$ given by

$$2K_x = 2\pi N \Delta F_x \text{ and } 2K_y = 2\pi N \Delta F_y \tag{45}$$

where $N$ is a power of 2 needed for the 2D IFFT.

From the so-obtained 2D sequence

$$\hat{F} = \hat{F}(i\ \Delta F_x, j\ \Delta F_y), \qquad \text{for } i, j = [-N, N], \tag{46}$$

we obtain the 2D periodic function $\hat{F}_p$:

$$\hat{F}_p = \hat{F}_p(i\ \Delta F_x, j\ \Delta F_y) \tag{47}$$

by periodically expanding $\hat{F}_p$ in both $i$ and $j$ with the same period $N$. We then apply the 2D IFFT to the first period of $\hat{F}_p$ multiplied by a scaling factor $\Delta F_x\ \Delta F_y$, and we get an estimate of the periodic discrete version of the function $f(x, y)$ of the form

$$\hat{f}_p(n\ \Delta X, m\ \Delta Y) = \text{2D IFFT}\ \{\Delta F_x\ \Delta F_y \hat{F}_p(i\ \Delta F_x, j\ \Delta F_y)\}, \quad \text{for } n, m, i, j = 0, 1, \cdots, N-1. \tag{48}$$

Following the inverse course, from (48), we get the function

$$\hat{f}(n\ \Delta X, m\ \Delta Y) \cong f(n\ \Delta X, m\ \Delta Y), \quad \text{for } n, m = -N/2 + 1 \text{ to } N/2 \tag{49}$$

where the estimate $\hat{f}$ of $f$ is equal to a period of $\hat{f}_p$ centered at the $(m, n) = (0, 0)$ point:

$$\hat{f}(n\ \Delta X, m\ \Delta Y) = \begin{cases} \hat{f}_p(n\ \Delta X, m\ \Delta Y), \\ \qquad \text{for } n, m = 0, 1, \cdots, N/2 \\ \hat{f}_p[(N-n)\ \Delta X, (N-m)\ \Delta Y], \\ \qquad \text{for } n,m = -1, -2, \cdots, -N/2 + 1 \\ 0, \quad \text{elsewhere.} \end{cases} \tag{50}$$

The main problem that appears is how one must choose the parameters $K_x$, $K_y$, and $N$ such that one can get a "good" estimate of the function $f(n\ \Delta X, m\ \Delta Y)$ and obtain, at the same time, an adequate resolution $\Delta X$ and $\Delta Y$ in the $x$ and $y$ space coordinates.

The function $\tilde{F}(\kappa_x, \kappa_y)$ in (38), (40), (42) is a product of the factor $H_0$, which is the transform of the input excitation current, and a factor which is the transfer function of the system. The $H_0$ factor is a 2D Bessel function with arguments related to the large $a$ and small $b$ semi-axes of the ellipse and to the wavenumbers $\kappa_x$, $\kappa_y$. In the examples presented in this paper, we have chosen $K_x$ and $K_y$ equal to $2\pi \times 400$. These values of $K_x$ and $K_y$ give a good resolution $\Delta X = \pi/K_x = 1/400$ and $\Delta Y = \pi K_y = 1/400$ of the IFT, and also a wide enough window $W$ for the Bessel functions. The second factor expressing the transfer function is independent of the excitation current and depends on the thickness and the electromagnetic constants of the slab. The bandwidth in $\kappa_x$ and $\kappa_y$ of this factor was found to be around $2\pi \times 40$, which is ten times less than the bandwidth of the excitation factor.

We are presenting four examples. In all four of them, the same geometry is maintained (Fig. 1), namely, a slab thickness $d = 2$ mm and a distance of excitation from slab $h = 10$ mm, so that comparisons could easily be made.

The excitation current is taken as an elliptical current with major semi-axis $a = 20$ mm and minor semi-axis $b = 10$ mm or a circular current of radius $R = 20$ mm, both with unit amplitude $I = 1$ A and at a frequency $f = 50$ Hz.

The material of the slab is chosen as aluminum, with relative permeability $\mu_r = 1$ and conductivity $\sigma = 3.54$

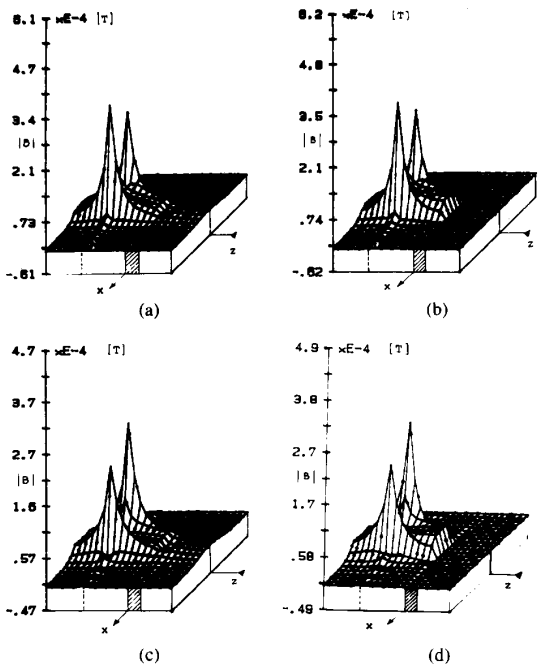


Fig. 2. Axonometric plot of $|B|$ versus $x$, $z$ for $y = 0$.

$\times 10^7$ S/m or silicon-iron steel, with relative permeability $\mu_r = 1000$ and conductivity $\sigma = 0.2 \times 10^7$ S/m.

We can thus classify the four examples as

a) aluminum slab with elliptical excitation
b) silicon-iron slab with elliptical excitation
c) aluminum slab with circular excitation
d) silicon-iron slab with circular excitation.

This numbering will be also followed in the figures presenting two-dimensional axonometric and contour plots of the magntiude of the magnetic flux density $|B|$ in various regions and of the magnitude of the eddy-current density $|J_3|$ inside the slab.

The first set of curves (Fig. 2) shows axonometric plots of the magnitude of magnetic induction $|B|$ for the four example cases all on the $x$-$z$ plane, cutting the excitation along the ellipse major axis or along a diameter in the case of circular excitation. Fig. 3 shows a contour plot of the same quantity as in Fig. 2, but for the case of aluminum slab with elliptical excitation since the contour plots for the rest of the cases are qualitatively similar. The contour plots of Fig. 4 again present the equiamplitude contour plots of $|B|$ for all four examples, but now for the region of interest around the slab. From all of these curves, it can be seen that $|B|$ presents a peak around the current and a steep gradient as we move from the current plane towards the slab surface. Its value decreases inside the slab having a smoother variation, and it is practically zero below the slab. This magnetic shielding effect is more clearly seen in Fig. 4, and as expected, is very strong in the case of a silicon-iron slab because of its high permeability. The maximum computed values of $|B|$ for the silicon-iron slab are about 50% lower than in the case of the aluminum slab.

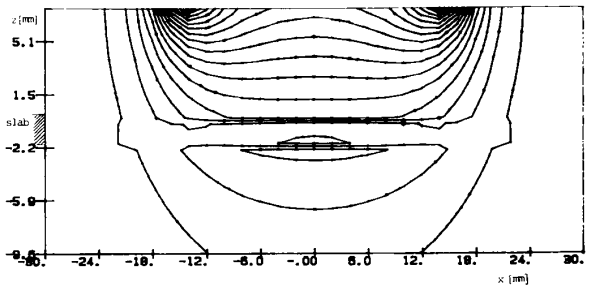


Fig. 3. Contour plot of $|B|$ versus $x$, $z$ for all $z$ and $y = 0$ for aluminum slab and elliptical excitation.

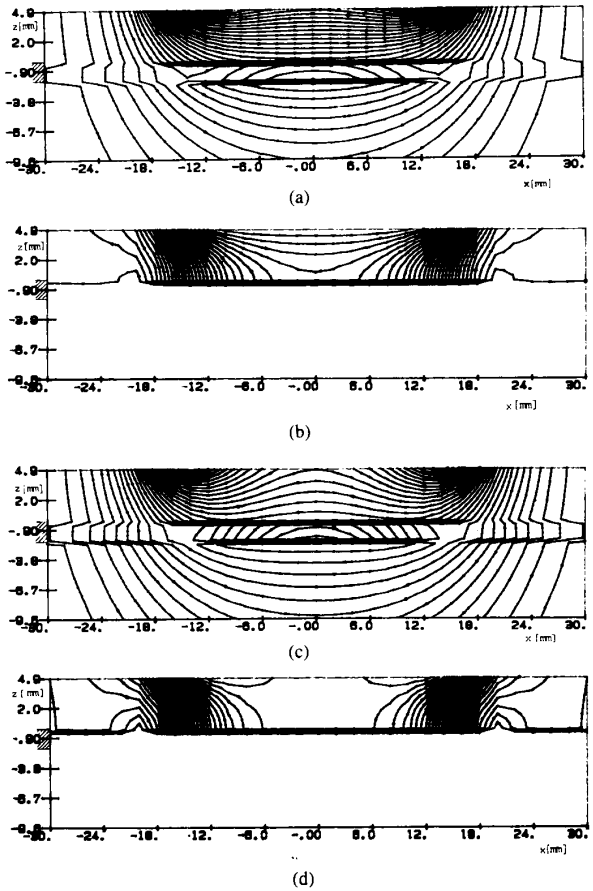


Fig. 4. Contour plots of $|B|$ versus $x$, $z$ for all $z$ and $y = 0$ in the region around the slab.

For the difference between the elliptical and circular excitation, we observe the following. In the case of the low-permeability aluminum slab and in the region below and inside the elliptical current loop, the equiamplitude curves of $|B|$ are almost parallel to the slab interface, both

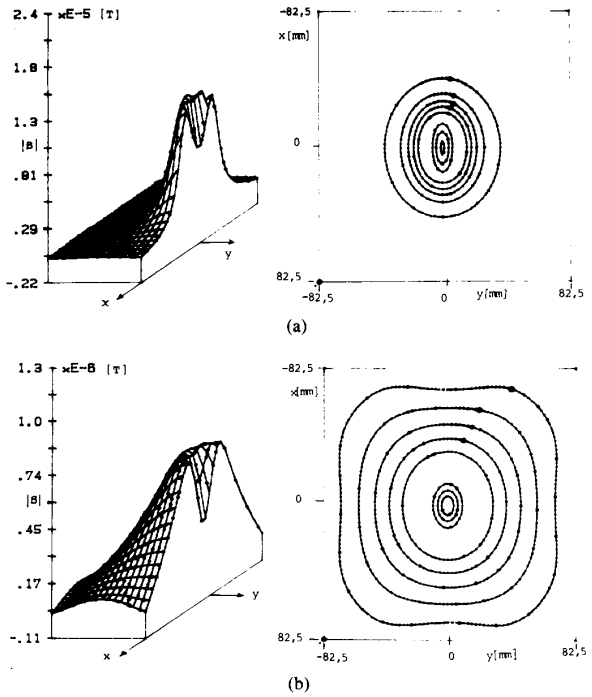


Fig. 5. Axonometric and contour plots of $|B|$ versus $x$, $y$ for $z = -0.81$ mm inside the slab.

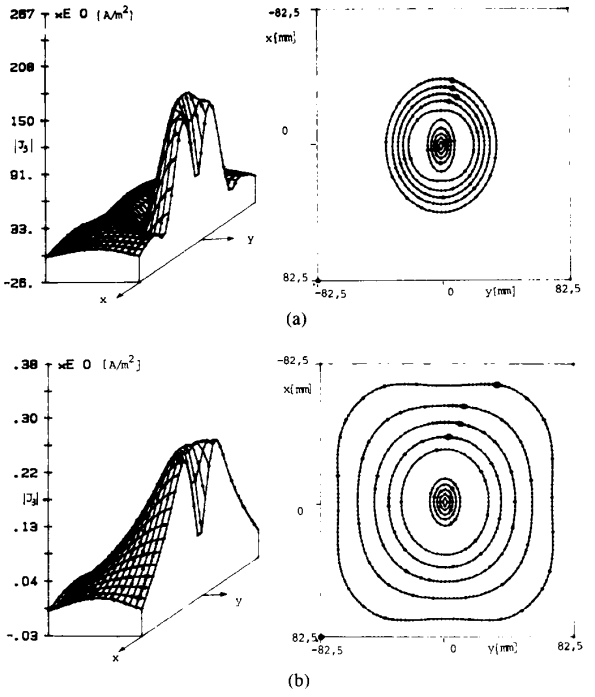


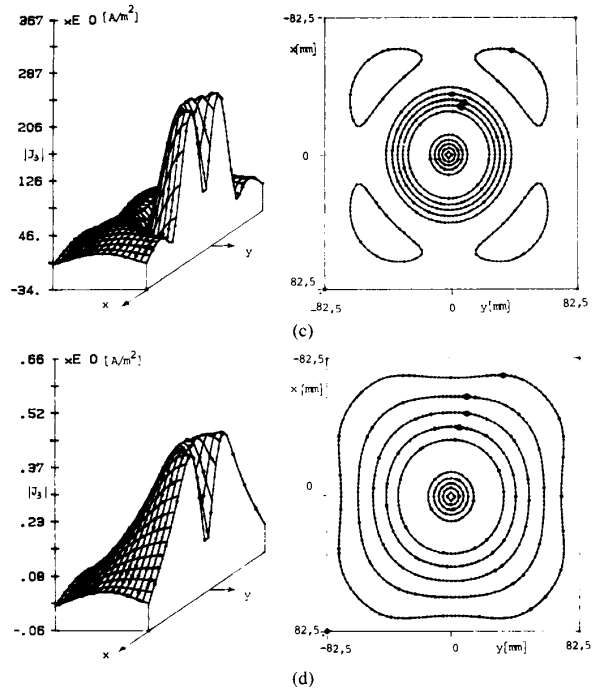


Fig. 6. Axonometric and contour plots of eddy currents $|J_3|$ versus $x$, $y$ inside the slab for $z = -0.81$ mm.

on the plane of the major axis and on the plane of the minor axis; while in the case of the circular loop, the field seems to be stronger just below the current filament. In the case of the high-permeability silicon–iron slab, this field concentration is even stronger, and, again, more explicit for the circular loop than the elliptical one.

For the elliptical loop excitation, the axonometric and contour plots of $|B|$ on the plane $z = -0.81$ mm (Fig. 5), which is on a plane parallel to the slab interface and almost at its middle, again show the peak at the current position and the expected symmetry of the computed values, which follow the shape of the current filament.

Finally, Fig. 6 shows the distribution of the eddy-current density magnitude $|J_3|$ on the same plane $z = -0.81$ mm inside the slab. The power loss curves have the same qualitative appearance with an appropriate change in scale. It is observed that the eddy-current contours again follow the shape of the current filament and take a circular form as they move away from the current loop. Any deviations are due to the numerical method. The values computed show that the eddy currents in the iron slab are about 700 times lower than in the aluminum slab in the case of the elliptical excitation, but only 500 times lower in the case of the circular excitation.

## VII. Conclusions

In this paper, the generation of eddy currents has been examined both analytically and numerically for the case of an elliptical current loop above and parallel to an infinite extent finite thickness conducting slab. The numerical results extracted agree well with theory. From the comparison between the elliptical and the circular exci-

tation, it has been observed that the circular excitation gives stronger, direction-independent fields, while the elliptical excitation gives rise to weaker but direction-dependent fields. Therefore, the elliptical loop could be used for nondestructive testing, probing, etc. The method used is general, and it can be easily extended to more complex forms of excitation or geometry (e.g., moving currents, multilayered media, superposition of excitation currents). The more general case of a current lying on a plane oblique to the slab surface also can be treated following the procedure outlined in the present paper. In that case, however, the excitation current FT will be more elaborate, and it would probably have to be carried out numerically.

## Appendix
## Evaluation of the 2D FT of the Excitation Current Components

From (27b), the $x$ component of the excitation current is

$$J_x = -I\,\delta(z-h)\Pi\left(\frac{x}{2a}\right)\left[\delta\left(y-\frac{b}{a}\sqrt{a^2-x^2}\right) - \delta\left(y+\frac{b}{a}\sqrt{a^2-x^2}\right)\right]. \tag{A.1}$$

The 2D FT of $J_x$ is given by

$$\tilde{J}_x = \int_{-\infty}^{+\infty}\int J_x e^{-jk_x x}e^{-jk_y y}\,dx\,dy. \tag{A.2}$$

Substituting (A.1) into (A.2) and using the shifting property of the delta function yields

$$\tilde{J}_x = -I\,\delta(z-h)\int_{-a}^{+a} e^{-jk_x x}\left[\exp\left(-jk_y\frac{b}{a}\sqrt{a^2-x^2}\right) - \exp\left(+jk_y\frac{b}{a}\sqrt{a^2-x^2}\right)\right]dx, \tag{A.3}$$

which is equivalent to the expression given in (29).

The integral in (A.3) is split into two integrals, differing only in the sign of the root. Making the change of variables

$$\cos\theta = \frac{x}{a} \tag{A.4}$$

with $0 \leqslant \theta \leqslant \pi$ in the first integral and $\pi \leqslant \theta \leqslant 2\pi$ in the second one, (A.3) becomes

$$\tilde{J}_x = I\,\delta(z-h)a\int_0^{2\pi}\exp\left[-j(ak_x\cos\theta + bk_y\sin\theta)\right]\cdot\sin\theta\,d\theta. \tag{A.5}$$

With the further substitutions

$$z = \sqrt{(ak_x)^2+(bk_y)^2}\quad \cos\varphi = \frac{ak_x}{z}\quad \sin\varphi = \frac{bk_y}{z}, \tag{A.6}$$

(A.5) is written as

$$\tilde{J}_x = -I\,\delta(z-h)j\tfrac{1}{2}a\left[\int_0^{2\pi}\exp\left[j\theta - jz\cos(\theta-\varphi)\right]d\theta - \int_0^{2\pi}\exp\left[j(-1)\theta - jz\cos(\theta-\varphi)\right]d\theta\right]. \tag{A.7}$$

For the Bessel functions, there holds the property

$$\int_0^{2\pi} e^{jn\theta - jz\cos(\theta-\varphi)}\,d\theta = (-j)^n e^{jn\varphi}2\pi J_n(z) \tag{A.8}$$

where $J_n(z)$ is the Bessel function of first kind and $n$th order.

Using (A.8) and the symmetric properties of Bessel functions, we have from (A.7)

$$\tilde{J}_x = -I\,\delta(z-h)j2\pi a J_1(z)\sin\varphi \tag{A.9a}$$

or, with a back substitution from (A.6) and (A.4),

$$\tilde{J}_x = -I\,\delta(z-h)j2\pi a\frac{bk_y}{\sqrt{(ak_x)^2+(bk_y)^2}}\cdot J_1\left(\sqrt{(ak_x)^2+(bk_y)^2}\right). \tag{A.9b}$$

Finally, using the recurrence properties of the Bessel functions, we get

$$\tilde{J}_x = -jk_y\pi abI\left[J_0\left(\sqrt{(ak_x)^2+(bk_y)^2}\right) + J_2\left(\sqrt{(ak_x)^2+(bk_y)^2}\right)\right]\delta(z-h). \tag{A.10}$$

Starting from (27a) and following the same line of analysis, we find for the 2D FT of the $y$ component of the excitation current

$$\tilde{J}_y = +jk_x\pi abI\left[J_0\left(\sqrt{(ak_x)^2+(bk_y)^2}\right) + J_2\left(\sqrt{(ak_x)^2+(bk_y)^2}\right)\right]\delta(z-h). \tag{A.11}$$

## References


[1] P. Hammond, "The calculation of the magnetic field of rotating machines," *Proc. IEE*, pp. 508-515, 1962.

[2] I. Woolley, "Eddy current losses in reactor flux shields," *Proc. IEE*, vol. 117, pp. 2142-2150, Nov. 1970.

[3] S. Panas and E. E. Kriezis, "Eddy current distribution due to a rectangular current frame moving above a conducting slab," *Arch. Elek.*, vol. 69, pp. 185-191, 1986.

[4] E. E. Kriezis and I. E. Xypteras, "Eddy current distribution and loss in a semi-infinite conducting space due to vertical current loop," *ETZ Arch.*, vol. 7, pp. 201-207, 1979.

[5] H. J. Tsaknakis and E. E. Kriezis, "Transient electromagnetic fields due to a circular current loop perpendicular or parallel to a conducting half-space," *IEEE Trans. Geosci. Remote Sensing*, vol. GE-20, pp. 122-130, 1982.

[6] ——, "Field distribution due to circular current loop placed at an arbitrary position above a conducting plate," *IEEE Trans. Geosci. Remote Sensing*, vol. GE-23, pp. 834–840, 1985.
[7] C. S. Antonopoulos and E. E. Kriezis, "Force on a parallel circular loop moving above a conducting slab and the eddy-current distribution," *Proc. IEE*, part A, vol. 133, no. 9, pp. 601–605, 1986.
[8] L. Hannakam, "Wirbelstrome in dunnen leitenden Platten Infolge bewegter stromfurdurchflossener Leiter," *Electrotech. Z. Ausg A*, vol. 86, no. 13, 1965.
[9] L. Hannakam and H.-D. Stahlmann, "Transienter Skineffect in einer dunnen Platte bei beliebiger Bewegung einer raumlichen Leiterscheife," *Archiv. Elek.*, pp. 47–61, 1981.
[10] W. Lord and R. Palanisamy, "Development of theoretical models for nondestructive testing eddy-current phenomena," *ASTM Special Tech. Publ. 722*, G. Birnbaum and G. Free, Ed. 1981, pp. 5–21.
[11] A. Papoulis, *Systems and Transforms with Applications in Optics*. New York: McGraw-Hill, 1968.
[12] D. S. Jones, *Generalized Functions*. London: McGraw-Hill, 1966.
[13] D. E. Dudgeon and R. M. Mersereau, *Multidimensional Digital Signal Processing*. Englewood Cliffs, NJ: Prentice-Hall, 1984.

**Stavros M. Panas** was born in Edessa, Greece, in 1946. He received the B.Sc. degree in physics from Aristotle University of Thessaloniki, Greece, in 1971, the M.Sc. degree in electrical engineering from the University of Oklahoma, Norman, in 1974, and the Ph.D. degree from Aristotle University of Thessaloniki, Greece, in 1983.

Since 1976 he has been with the School of Electrical Engineering, Aristotle University of Thessaloniki, Greece, where he is now an Assistant Professor. His areas of interest are eddy currents, electromagnetic fields, signal processing, and applications in biomedical engineering.

**Antonis G. Papayiannakis** was born in Thessaloniki, Greece, in 1954. He received the Diploma in electrical engineering in 1977 and the Ph.D. degree in 1986 from the Schoool of Electrical Engineering, Aristotle University of Thessaloniki, Greece.

He has been with the University since 1980. His present position is Lecturer, and he is teaching electromagnetic field theory and optics. His areas of interest cover the fields of electromagnetic wave propagation and scattering, classical and fiber optics, Green's functions, and the method of moments.